

The homogenization of orthorhombic piezoelectric composites by the strong–property–fluctuation theory

Andrew J. Duncan¹, Tom G. Mackay²

*School of Mathematics and Maxwell Institute for Mathematical Sciences
University of Edinburgh, Edinburgh EH9 3JZ, UK*

Akhlesh Lakhtakia³

*NanoMM — Nanoengineered Metamaterials Group
Department of Engineering Science and Mechanics
Pennsylvania State University, University Park, PA 16802–6812, USA*

Abstract

The linear strong–property–fluctuation theory (SPFT) was developed in order to estimate the constitutive parameters of certain homogenized composite materials (HCMs) in the long–wavelength regime. The component materials of the HCM were generally orthorhombic $mm2$ piezoelectric materials, which were randomly distributed as oriented ellipsoidal particles. At the second–order level of approximation, wherein a two–point correlation function and its associated correlation length characterize the component material distributions, the SPFT estimates of the HCM constitutive parameters were expressed in terms of numerically–tractable two–dimensional integrals. Representative numerical calculations revealed that: (i) the lowest–order SPFT estimates are qualitatively similar to those provided by the corresponding Mori–Tanaka homogenization formalism, but differences between the two estimates become more pronounced as the component particles become more eccentric in shape; and (ii) the second–order SPFT estimate provides a significant correction to the lowest–order estimate, which reflects dissipative losses due to scattering.

Keywords: Homogenization, strong–property–fluctuation theory, metamaterials, Mori–Tanaka formalism, orthorhombic piezoelectric.

1 Introduction

Since piezoelectric materials can convert electrical energy to mechanical energy, and vice versa, they are of considerable technological importance. However, bulk piezoelectric materials commonly exhibit physical properties which render them unsuitable for particular applications. For example, certain ceramics exhibit strong piezoelectric properties but their weight, malleability and acoustic impedance are not suitable for transducer applications [1]. Accordingly, composite piezoelectric materials are often more technologically attractive [2]; and these can be found in a host of applications such as in transducers, sensors, actuators and energy harvesting devices, for example [3, 4]. Furthermore, the recent proliferation of multifunctional metamaterials [5] — which often take the form of homogenized composite materials (HCMs), exhibiting exotic constitutive properties [6] — presents interesting possibilities for piezoelectric HCMs.

While the estimation of elastodynamic or electromagnetic constitutive parameters of HCMs is a challenging task, especially for anisotropic HCMs, the estimation of constitutive parameters of piezoelectric HCMs is more challenging due to the coupling of elastodynamic and electromagnetic fields. Numerous homogenization formalisms have been proposed for piezoelectric HCMs, many of which build upon Eshelby’s landmark

¹Corresponding author. E–mail: Andrew.Duncan@ed.ac.uk.

²E–mail: T.Mackay@ed.ac.uk.

³E–mail: akhlesh@psu.edu

description of the elastodynamic response of a single ellipsoidal particle immersed in an infinite homogeneous medium [7, 8]. For example, the Mori–Tanaka [9, 10, 11], self-consistent and differential approaches [12] — and combinations of these [13] — feature prominently in the literature. In the following we present a fundamentally different approach to estimating the constitutive properties of piezoelectric HCMs, based on the strong-property-fluctuation theory (SPFT). A key feature of the SPFT homogenization approach — which distinguishes it from other more conventional approaches — is the accommodation of higher-order characterizations of the distributional statistics of the HCM’s component materials.

The origins of the SPFT lie in wave propagation studies for continuously random mediums [14]. It was later adapted to estimate the electromagnetic [15, 16, 17], acoustic [18] and elastodynamic [19] constitutive parameters of HCMs. Within the SPFT, the estimation the HCMs constitutive parameters arises by successive refinements to the constitutive parameters of a homogeneous comparison medium. Iterations are expressed in terms of correlation functions describing the spatial distributions of the component materials. In principle, correlation functions of arbitrarily high-order may be incorporated; but, in practice, the SPFT is most often implemented at the second-order level of approximation, wherein a two-point correlation function and its associated correlation length characterize the component material distributions.

We establish here the linear, second-order SPFT appropriate to orthorhombic $mm2$ piezoelectric HCMs, arising from component materials which are randomly distributed as oriented ellipsoidal particles. The theoretical development builds upon the corresponding development of the orthotropic elastodynamic SPFT [19, 20]. A representative numerical example is used to illustrate the theory, and results are compared with those from the well-established Mori–Tanaka formalism.

2 Theory

2.1 Preliminaries

In the following, we consider piezoelectric materials described by constitutive relations of the form [21, 22]

$$\left. \begin{aligned} \sigma_{ab} &= C_{abmn}S_{mn} - e_{nab}E_n \\ D_a &= e_{amn}S_{mn} + \epsilon_{an}E_n \end{aligned} \right\}, \quad (1)$$

wherein the elastic strain S_{mn} and the electric field E_n are taken as independent variables, which are related to the stress σ_{ab} and dielectric displacement D_a via the elastic stiffness tensor C_{abmn} (measured in a constant electric field), the piezoelectric tensor e_{nab} (measured at a constant strain or electric field), and the dielectric tensor ϵ_{an} (measured at a constant strain). Here, and hereafter, tensors are represented in plain font and lowercase tensor indexes range from 1 to 3, with a repeated index implying summation.

We develop the SPFT in the frequency domain. Accordingly the complex-valued representations of the stress, strain and electromagnetic fields have an implicit $\exp(-i\omega t)$ dependency on time t , with ω being the angular frequency and $i = \sqrt{-1}$. The possibility of dissipative behaviour is thereby accommodated via the imaginary parts of complex-valued constitutive parameters.

The constitutive relations (1) are more conveniently expressed in the symbolic form

$$\check{\sigma}_{aB} = \check{C}_{aBMn}\check{S}_{Mn}, \quad (2)$$

where the extended stress symbol

$$\check{\sigma}_{aB} = \begin{cases} \sigma_{ab}, & B = b = 1, 2, 3 \\ D_a, & B = 4 \end{cases}, \quad (3)$$

the extended stiffness symbol

$$\check{C}_{aBMn} = \begin{cases} C_{abmn}, & B = b = 1, 2, 3; M = m = 1, 2, 3 \\ e_{nab}, & B = b = 1, 2, 3; M = 4 \\ -e_{amn}, & B = 4; M = m = 1, 2, 3 \\ \epsilon_{an}, & B, M = 4 \end{cases}, \quad (4)$$

and the extended strain symbol

$$\check{S}_{Mn} = \begin{cases} S_{mn}, & M = m = 1, 2, 3 \\ E_n, & M = 4 \end{cases}. \quad (5)$$

Here, and hereafter, uppercase indexes range from 1 to 4. Note that the extended quantities defined in eqs. (3), (4) and (5) are not tensors — these are simply symbols which are introduced to allow a compact representation of the piezoelectric constitutive relations [10].

In developing the SPFT appropriate to piezoelectric HCMs, it is expedient to express the constitutive relations (2) in matrix–vector form as

$$\check{\boldsymbol{\sigma}} = \check{\underline{\underline{\mathbf{C}}}} \cdot \check{\underline{\underline{\mathbf{S}}}}, \quad (6)$$

wherein $\check{\boldsymbol{\sigma}}$ and $\check{\underline{\underline{\mathbf{S}}}}$ are column 12–vectors representing the extended stress and extended strain symbols, respectively, and $\check{\underline{\underline{\mathbf{C}}}}$ is a 12×12 matrix which represents the extended stiffness symbol. Here, and hereafter, matrixes are denoted by double underlining and bold font, whereas vectors are in bold font with no underlining. For use later on, we note that the pq th entry of a matrix $\underline{\underline{\mathbf{A}}}$ is written as $[\underline{\underline{\mathbf{A}}}]_{pq}$, while the p th entry of a vector \mathbf{b} is written as $[\mathbf{b}]_p$. Accordingly, the matrix entry $[\underline{\underline{\mathbf{A}}} \cdot \underline{\underline{\mathbf{B}}}]_{pr} = [\underline{\underline{\mathbf{A}}}]_{pq} [\underline{\underline{\mathbf{B}}}]_{qr}$, the vector entry $[\underline{\underline{\mathbf{A}}} \cdot \mathbf{b}]_p = [\underline{\underline{\mathbf{A}}}]_{pq} [\mathbf{b}]_q$, and the scalar $\mathbf{a} \cdot \mathbf{b} = [\mathbf{a}]_p [\mathbf{b}]_p$. The adjoint, determinant, inverse, trace and transpose of a matrix $\underline{\underline{\mathbf{A}}}$ are denoted by $\text{adj}(\underline{\underline{\mathbf{A}}})$, $\det(\underline{\underline{\mathbf{A}}})$, $\underline{\underline{\mathbf{A}}}^{-1}$, $\text{tr}(\underline{\underline{\mathbf{A}}})$ and $\underline{\underline{\mathbf{A}}}^T$, respectively. The $n \times n$ null matrix is written as $\underline{\underline{\mathbf{0}}}_{n \times n}$.

Our concern in this article is with orthorhombic $mm2$ piezoelectric materials [21, 22]. For this symmetry class, the extended stiffness matrix has the block matrix form

$$\check{\underline{\underline{\mathbf{C}}}} = \begin{pmatrix} \underline{\underline{\mathbf{C}}} & -\underline{\underline{\mathbf{e}}}^T \\ \underline{\underline{\mathbf{e}}} & \underline{\underline{\boldsymbol{\epsilon}}} \end{pmatrix}, \quad (7)$$

where the 9×9 stiffness matrix $\underline{\underline{\mathbf{C}}}$ may be expressed as

$$\underline{\underline{\mathbf{C}}} = \begin{pmatrix} \underline{\underline{\mathbf{C}}}_a & \underline{\underline{\mathbf{0}}}_{3 \times 3} & \underline{\underline{\mathbf{0}}}_{3 \times 3} \\ \underline{\underline{\mathbf{0}}}_{3 \times 3} & \underline{\underline{\mathbf{C}}}_b & \underline{\underline{\mathbf{C}}}_b \\ \underline{\underline{\mathbf{0}}}_{3 \times 3} & \underline{\underline{\mathbf{C}}}_b & \underline{\underline{\mathbf{C}}}_b \end{pmatrix}, \quad (8)$$

with the 3×3 symmetric matrix components

$$\underline{\underline{\mathbf{C}}}_a = \begin{pmatrix} C_{11} & C_{12} & C_{13} \\ C_{12} & C_{22} & C_{23} \\ C_{13} & C_{23} & C_{33} \end{pmatrix}, \quad \underline{\underline{\mathbf{C}}}_b = \begin{pmatrix} C_{44} & 0 & 0 \\ 0 & C_{55} & 0 \\ 0 & 0 & C_{66} \end{pmatrix}; \quad (9)$$

while the 9×3 piezoelectric matrix $\underline{\underline{\mathbf{e}}}$ may be expressed as

$$\underline{\underline{\mathbf{e}}} = \begin{pmatrix} 0 & 0 & 0 & 0 & e_{15} & 0 & 0 & e_{15} & 0 \\ 0 & 0 & 0 & e_{24} & 0 & 0 & e_{24} & 0 & 0 \\ e_{31} & e_{32} & e_{33} & 0 & 0 & 0 & 0 & 0 & 0 \end{pmatrix} \quad (10)$$

and the 3×3 dielectric matrix $\underline{\underline{\boldsymbol{\epsilon}}}$ as

$$\underline{\underline{\boldsymbol{\epsilon}}} = \begin{pmatrix} \epsilon_{11} & 0 & 0 \\ 0 & \epsilon_{22} & 0 \\ 0 & 0 & \epsilon_{33} \end{pmatrix}. \quad (11)$$

The correspondence between the tensor/extended symbol representation and the matrix–vector representation is described in Appendix A.

In an analogous fashion, the material density ρ may be represented via the extended density symbol

$$\check{\rho}_{BM} = \begin{cases} \rho, & B = M = 1, 2, 3 \\ 0, & \text{otherwise} \end{cases}, \quad (12)$$

which has the 4×4 extended matrix counterpart $\check{\underline{\underline{\rho}}}$ with entries

$$\left[\check{\underline{\underline{\rho}}} \right]_{MP} = \check{\rho}_{MP}. \quad (13)$$

2.2 Component materials

We consider the homogenization of a composite comprising two component materials, labelled as component material ‘1’ and component material ‘2’. In general, both components are homogeneous, orthorhombic $mm2$ piezoelectric materials, characterized by the stiffness tensors $C_{abmn}^{(\ell)}$, piezoelectric tensors $e_{nab}^{(\ell)}$, dielectric tensors $\epsilon_{an}^{(\ell)}$ and densities $\rho^{(\ell)}$ ($\ell = 1, 2$). In conformity with the notational practices introduced in §2.1, the component materials are also described by the extended stiffness symbols $\check{C}_{aBMn}^{(\ell)}$ (and their 12×12 matrix equivalents $\check{\underline{\underline{C}}}^{(\ell)}$) and extended density symbols $\check{\rho}_{BM}^{(\ell)}$ (and their 4×4 matrix equivalents $\check{\underline{\underline{\rho}}}^{(\ell)}$).

The component materials are randomly distributed as identically-oriented, conformal, ellipsoidal particles. The principal axes of the ellipsoidal particles are aligned with the Cartesian axes. Thus, the surface of each ellipsoidal particle may be parameterized by the vector

$$\mathbf{r}^{(e)} = \eta \underline{\underline{\mathbf{U}}} \cdot \hat{\mathbf{r}}, \quad (14)$$

where η is a linear measure of size, $\hat{\mathbf{r}}$ is the radial unit vector and the diagonal shape matrix

$$\underline{\underline{\mathbf{U}}} = \frac{1}{\sqrt[3]{abc}} \begin{pmatrix} a & 0 & 0 \\ 0 & b & 0 \\ 0 & 0 & c \end{pmatrix}, \quad (a, b, c \in \mathbb{R}^+). \quad (15)$$

Let V denote the space occupied by the composite material. Then $V = V^{(1)} \cup V^{(2)}$ where $V^{(1)}$ and $V^{(2)}$ contain the two component materials labelled as ‘1’ and ‘2’, respectively, and $V^{(1)} \cap V^{(2)} = \emptyset$. The distributional statistics of the component materials are described in terms of moments of the characteristic functions

$$\Phi^{(\ell)}(\mathbf{r}) = \begin{cases} 1, & \mathbf{r} \in V^{(\ell)}, \\ 0, & \mathbf{r} \notin V^{(\ell)}, \end{cases} \quad (\ell = 1, 2). \quad (16)$$

The first statistical moment of $\Phi^{(\ell)}$, i.e.,

$$\langle \Phi^{(\ell)}(\mathbf{r}) \rangle = f^{(\ell)}, \quad (\ell = 1, 2), \quad (17)$$

delivers the volume fraction of component material ℓ , which is subject to the constraint $\sum_{\ell=1}^2 f^{(\ell)} = 1$. The

second statistical moment of $\Phi^{(\ell)}$ constitutes a two-point covariance function. Investigations involving the electromagnetic SPFT have demonstrated that the specific form of the covariance function has only a minor influence on estimates of HCM constitutive parameters, for a range of physically-plausible covariance functions [25]. Here we adopt the physically-motivated form [26]

$$\langle \Phi^{(\ell)}(\mathbf{r}) \Phi^{(\ell)}(\mathbf{r}') \rangle = \begin{cases} \langle \Phi^{(\ell)}(\mathbf{r}) \rangle \langle \Phi^{(\ell)}(\mathbf{r}') \rangle, & |\underline{\underline{\mathbf{U}}}^{-1} \cdot (\mathbf{r} - \mathbf{r}')| > L \\ \langle \Phi^{(\ell)}(\mathbf{r}) \rangle, & |\underline{\underline{\mathbf{U}}}^{-1} \cdot (\mathbf{r} - \mathbf{r}')| \leq L \end{cases}, \quad (18)$$

which has been widely used in electromagnetic and elastodynamic SPFT studies. The correlation length L in eq. (18) is required to be much smaller than the associated piezoelectric wavelengths, but larger than the particle size parameter η .

2.3 Comparison material

A homogeneous comparison material provides the initial ansatz for an iterative procedure that delivers a succession of SPFT estimates of the HCM constitutive parameters [19]. Accordingly, the comparison material represents the lowest-order SPFT estimate of the HCM. In consonance with the component materials, the comparison material is an orthorhombic $mm2$ piezoelectric material, in general. The piezoelectric constitutive properties of this orthorhombic comparison material (OCM) are encapsulated by its extended stiffness symbol $\check{C}_{lMPq}^{(ocm)}$ (and its 12×12 matrix equivalent $\underline{\check{C}}^{(ocm)}$) and extended density symbol $\check{\rho}_{MP}^{(ocm)}$ (and its 4×4 matrix equivalent $\underline{\check{\rho}}^{(ocm)}$).

In order to establish the spectral Green function for the OCM — which is a key element in the SPFT formulation — we first consider the corresponding extended equation of motion. This may be written in the frequency domain as [27]

$$\check{C}_{lMPq}^{(ocm)} \partial_l \partial_q \check{u}_P + \omega^2 \check{u}_M = -\check{F}_M, \quad (19)$$

where the extended displacement

$$\check{u}_M = \begin{cases} u_m, & M = m = 1, 2, 3 \\ \Phi, & P = 4 \end{cases} \quad (20)$$

combines the displacement u_m and electric scalar potential Φ , and the extended body force

$$\check{F}_M = \begin{cases} F_m, & M = m = 1, 2, 3 \\ -q, & M = 4 \end{cases} \quad (21)$$

combines the body force F_m and the electric charge q . Accordingly, the sought after spectral Green function for the OCM emerges as the 4×4 matrix

$$\underline{\mathbf{G}}^{(ocm)}(\mathbf{k}) = [k^2 \underline{\mathbf{a}}(\hat{\mathbf{k}}) - \omega^2 \underline{\check{\rho}}^{(ocm)}]^{-1}, \quad (22)$$

where the 4×4 matrix $\underline{\mathbf{a}}(\hat{\mathbf{k}})$ has entries

$$\left[\underline{\mathbf{a}}(\hat{\mathbf{k}}) \right]_{MP} = \frac{k_s \check{C}_{sMPq}^{(ocm)} k_q}{k^2}. \quad (23)$$

Herein, $\mathbf{k} = k\hat{\mathbf{k}} \equiv (k_1, k_2, k_3)$ with $\hat{\mathbf{k}} = (\sin \theta \cos \phi, \sin \theta \sin \phi, \cos \theta)$.

The OCM extended constitutive symbols $\check{C}_{lMPq}^{(ocm)}$ and $\check{\rho}_{MP}^{(ocm)}$ are derived via the imposition of the two conditions [19, eqs. (2.72), (2.73)]

$$\langle \Phi^{(1)}(\mathbf{r}) \xi_{lMPq}^{(1)} + \Phi^{(2)}(\mathbf{r}) \xi_{lMPq}^{(2)} \rangle = 0, \quad (24)$$

$$\langle \Phi^{(1)}(\mathbf{r}) \left[\check{\rho}^{(1)} - \check{\rho}^{(ocm)} \right]_{MP} + \Phi^{(2)}(\mathbf{r}) \left[\check{\rho}^{(2)} - \check{\rho}^{(ocm)} \right]_{MP} \rangle = 0, \quad (25)$$

which is necessary to remove certain secular terms. In eq. (24), the quantities

$$\xi_{lMPq}^{(\ell)} = \left(\check{C}_{lMSt}^{(\ell)} - \check{C}_{lMSt}^{(ocm)} \right) \eta_{StPq}^{(\ell)}, \quad (\ell = 1, 2), \quad (26)$$

where $\eta_{StPq}^{(\ell)}$ is given implicitly through

$$\check{S}_{Pq}^{(\ell)} = \eta_{PqSt}^{(\ell)} \check{f}_{St}^{(\ell)}, \quad (27)$$

$$\check{f}_{Tj}^{(\ell)} = \check{S}_{Tj}^{(\ell)} + W_{TjIM} \left(\check{C}_{lMPq}^{(\ell)} - \check{C}_{lMPq}^{(ocm)} \right) \check{S}_{Pq}^{(\ell)}, \quad (28)$$

with the renormalization tensor

$$W_{PstU} = \begin{cases} \frac{1}{8\pi} \int_0^{2\pi} d\phi \int_0^\pi d\theta \frac{\sin \theta}{(\underline{\mathbf{U}}^{-1} \cdot \hat{\mathbf{k}}) \cdot (\underline{\mathbf{U}}^{-1} \cdot \hat{\mathbf{k}})} \times \\ \left\{ (\underline{\mathbf{U}}^{-1} \cdot \hat{\mathbf{k}})_t \left\{ (\underline{\mathbf{U}}^{-1} \cdot \hat{\mathbf{k}})_s [\underline{\mathbf{a}}^{-1}(\underline{\mathbf{U}}^{-1} \cdot \hat{\mathbf{k}})]_{pU} \right. \right. \\ \left. \left. + (\underline{\mathbf{U}}^{-1} \cdot \hat{\mathbf{k}})_p [\underline{\mathbf{a}}^{-1}(\underline{\mathbf{U}}^{-1} \cdot \hat{\mathbf{k}})]_{sU} \right\}, \right. & \text{P} = \text{p} = 1, 2, 3 \quad \cdot \quad (29) \\ \left. \frac{1}{8\pi} \int_0^{2\pi} d\phi \int_0^\pi d\theta \sin \theta \frac{(\underline{\mathbf{U}}^{-1} \cdot \hat{\mathbf{k}})_t (\underline{\mathbf{U}}^{-1} \cdot \hat{\mathbf{k}})_s [\underline{\mathbf{a}}^{-1}(\underline{\mathbf{U}}^{-1} \cdot \hat{\mathbf{k}})]_{pU}}{(\underline{\mathbf{U}}^{-1} \cdot \hat{\mathbf{k}}) \cdot (\underline{\mathbf{U}}^{-1} \cdot \hat{\mathbf{k}})}, \right. & \text{P} = 4 \end{cases}$$

Upon substituting eqs. (26)–(28) into eq. (24), exploiting eq. (17), and after some algebraic manipulations, we obtain

$$f^{(1)} \left[\left(\underline{\check{\mathbf{C}}}^{(1)} - \underline{\check{\mathbf{C}}}^{(ocm)} \right)^\dagger + \underline{\mathbf{W}} \right]^\dagger + f^{(2)} \left[\left(\underline{\check{\mathbf{C}}}^{(2)} - \underline{\check{\mathbf{C}}}^{(ocm)} \right)^\dagger + \underline{\mathbf{W}} \right]^\dagger = \underline{\mathbf{0}}_{12 \times 12}, \quad (30)$$

wherein the 12×12 matrix equivalent of W_{RstU} (namely, $\underline{\mathbf{W}}$) has been introduced and † denotes the matrix operation defined in Appendix A. The OCM stiffness matrix may be extracted from (30) as

$$\underline{\check{\mathbf{C}}}^{(ocm)} = \underline{\check{\mathbf{C}}}^{(1)} + f^{(2)} \left[\underline{\boldsymbol{\tau}} + \left(\underline{\check{\mathbf{C}}}^{(2)} - \underline{\check{\mathbf{C}}}^{(ocm)} \right) \cdot \underline{\mathbf{W}} \right]^\dagger \cdot \left(\underline{\check{\mathbf{C}}}^{(1)} - \underline{\check{\mathbf{C}}}^{(2)} \right), \quad (31)$$

where $\underline{\boldsymbol{\tau}}$ is the 12×12 matrix representation of the extended identity $\tau_{rSTu} = \tau_{RstU}$, as described in Appendix A. By standard numerical procedures, such as the Jacobi method [28], the nonlinear relation (31) is solved for $\underline{\check{\mathbf{C}}}^{(ocm)}$.

After combining eq. (17) with eq. (25), it follows immediately that the OCM density is the volume average of the densities of the component materials ‘1’ and ‘2’; i.e.,

$$\underline{\check{\rho}}^{(ocm)} = f^{(1)} \underline{\check{\rho}}^{(1)} + f^{(2)} \underline{\check{\rho}}^{(2)}. \quad (32)$$

2.4 Second-order SPFT

Building upon the corresponding results for the elastodynamic SPFT [19], the second-order⁴ estimates of the HCM extended stiffness and density symbols may be expressed in terms of three-dimensional integrals as

$$\begin{aligned} \check{C}_{lMPq}^{(spft)} &= \check{C}_{lMPq}^{(ocm)} - \frac{\omega^2}{2} \int d^3k \frac{k_t}{k^2} B_{tUPq}^{lMrs}(\mathbf{k}) \left[\underline{\check{\rho}}^{(ocm)} \right]_{XY} \left[\underline{\mathbf{G}}^{(ocm)}(\mathbf{k}) \right]_{YU} \times \\ &\quad \left\{ k_s \left[\underline{\mathbf{a}}^{-1}(\hat{\mathbf{k}}) \right]_{rX} + k_r \left[\underline{\mathbf{a}}^{-1}(\hat{\mathbf{k}}) \right]_{sX} \right\} - \\ &\quad \frac{\omega^2}{2} \int d^3k \frac{k_t}{k^2} B_{tUPq}^{lM4s}(\mathbf{k}) \left[\underline{\check{\rho}}^{(ocm)} \right]_{XY} \left[\underline{\mathbf{G}}^{(ocm)}(\mathbf{k}) \right]_{YU} \left\{ k_s \left[\underline{\mathbf{a}}^{-1}(\hat{\mathbf{k}}) \right]_{4X} \right\} \end{aligned} \quad (33)$$

and

$$\check{\rho}_{MP}^{(spft)} = \check{\rho}_{MP}^{(ocm)} + \omega^2 \int d^3k B_{MSUP}(\mathbf{k}) \left[\underline{\mathbf{G}}^{(ocm)}(\mathbf{k}) \right]_{SU}. \quad (34)$$

⁴The first-order SPFT estimate is identical to the zeroth-order SPFT estimate which is represented by the comparison material.

The symbols $B_{tUPq}^{lMRs}(\mathbf{k})$ and $B_{MSUP}(\mathbf{k})$ represent the spectral covariance functions given as

$$\left. \begin{aligned} B_{tUPq}^{lMRs}(\mathbf{k}) &= \frac{\left(\xi_{lMNs}^{(2)} - \xi_{lMNs}^{(1)}\right) \left(\xi_{tUPq}^{(2)} - \xi_{tUPq}^{(1)}\right)}{8\pi^3} \int d^3R \Gamma(\mathbf{R}) \exp(-i\mathbf{k} \cdot \mathbf{R}) \\ B_{MSUP}(\mathbf{k}) &= \frac{\left(\rho_{MS}^{(2)} - \rho_{MS}^{(1)}\right) \left(\rho_{UP}^{(2)} - \rho_{UP}^{(1)}\right)}{8\pi^3} \int d^3R \Gamma(\mathbf{R}) \exp(-i\mathbf{k} \cdot \mathbf{R}) \end{aligned} \right\}, \quad (35)$$

with

$$\begin{aligned} \Gamma(\mathbf{R}) = \Gamma(\mathbf{r} - \mathbf{r}') &= \langle \Phi^{(1)}(\mathbf{r}) \Phi^{(1)}(\mathbf{r}') \rangle - \langle \Phi^{(1)}(\mathbf{r}) \rangle \langle \Phi^{(1)}(\mathbf{r}') \rangle \\ &\equiv \langle \Phi^{(2)}(\mathbf{r}) \Phi^{(2)}(\mathbf{r}') \rangle - \langle \Phi^{(2)}(\mathbf{r}) \rangle \langle \Phi^{(2)}(\mathbf{r}') \rangle. \end{aligned} \quad (36)$$

In order to make the integrals in the expressions for $\check{C}_{lMPq}^{(spft)}$ and $\check{\rho}_{MP}^{(spft)}$ presented in eqs. (33) and (34) numerically tractable, we simplify them as follows. Let us begin with the integral on the right sides of eqs. (35). Upon implementing the step function-shaped covariance function (18), we find

$$\int d^3R \Gamma(\mathbf{R}) \exp(-i\mathbf{k} \cdot \mathbf{R}) = \int_{|\mathbf{R}| \leq L} d^3R \exp[-i(\underline{\mathbf{U}} \cdot \mathbf{k}) \cdot \mathbf{R}]. \quad (37)$$

Thereby, the expressions for $B_{tUPq}^{lMRs}(\mathbf{k})$ and $B_{MSUP}(\mathbf{k})$ reduce to

$$\left. \begin{aligned} B_{tUPq}^{lMRs}(\mathbf{k}) &= \frac{f^{(1)} f^{(2)} \left(\xi_{lMRs}^{(2)} - \xi_{lMRs}^{(1)}\right) \left(\xi_{tUPq}^{(2)} - \xi_{tUPq}^{(1)}\right)}{2(\pi k \sigma)^2} \left[\frac{\sin(k\sigma L)}{k\sigma} - L \cos(k\sigma L) \right] \\ B_{MSUP}(\mathbf{k}) &= \frac{f^{(1)} f^{(2)} \left(\rho_{MS}^{(2)} - \rho_{MS}^{(1)}\right) \left(\rho_{UP}^{(2)} - \rho_{UP}^{(1)}\right)}{2(\pi k \sigma)^2} \left[\frac{\sin(k\sigma L)}{k\sigma} - L \cos(k\sigma L) \right] \end{aligned} \right\}, \quad (38)$$

wherein the scalar function

$$\sigma \equiv \sigma(\theta, \phi) = \sqrt{a^2 \sin^2 \theta \cos^2 \phi + b^2 \sin^2 \theta \sin^2 \phi + c^2 \cos^2 \theta} \quad (39)$$

is introduced.

Now we turn to the integrals in (33) and (34). In analogy with the corresponding expression for the elastodynamic SPFT [20], the spectral Green function $\underline{\mathbf{G}}^{(ocm)}(\mathbf{k})$ may be conveniently expressed as

$$\underline{\mathbf{G}}^{(ocm)}(\mathbf{k}) = \frac{\underline{\mathbf{D}}(\mathbf{k})}{\Delta(\mathbf{k})}, \quad (40)$$

where the 4×4 matrix function

$$\underline{\mathbf{D}}(\mathbf{k}) = \text{adj} \left[k^2 \underline{\mathbf{a}}(\hat{\mathbf{k}}) - \omega^2 \underline{\check{\rho}}^{(ocm)} \right] \quad (41)$$

and the scalar function

$$\begin{aligned} \Delta(k) &= k^8 \det \left[\underline{\mathbf{a}}(\hat{\mathbf{k}}) \right] - \text{tr} \left\{ \text{adj} \left[k^2 \underline{\mathbf{a}}(\hat{\mathbf{k}}) \right] \cdot \omega^2 \underline{\check{\rho}}^{(ocm)} \right\} - k^2 \text{tr} \left[\text{adj}(\omega^2 \underline{\check{\rho}}^{(ocm)}) \cdot \underline{\mathbf{a}}(\hat{\mathbf{k}}) \right] \\ &+ k^4 \left(\text{tr} \left\{ \left[\underline{\mathbf{a}}(\hat{\mathbf{k}}) \right]_{44} \left[\underline{\check{\rho}}^\#(\hat{\mathbf{k}}) \cdot \text{adj}(\omega^2 \underline{\check{\rho}}^\#) \right] \right\} - \left[\underline{\mathbf{a}}(\hat{\mathbf{k}}) \right]_{41} \left[\underline{\mathbf{a}}(\hat{\mathbf{k}}) \right]_{14} \left[\text{adj}(\omega^2 \underline{\check{\rho}}^\#) \right]_{11} \right. \\ &\left. - \left[\underline{\mathbf{a}}(\hat{\mathbf{k}}) \right]_{42} \left[\underline{\mathbf{a}}(\hat{\mathbf{k}}) \right]_{24} \left[\text{adj}(\omega^2 \underline{\check{\rho}}^\#) \right]_{22} - \left[\underline{\mathbf{a}}(\hat{\mathbf{k}}) \right]_{31} \left[\underline{\mathbf{a}}(\hat{\mathbf{k}}) \right]_{13} \left[\text{adj}(\omega^2 \underline{\check{\rho}}^\#) \right]_{33} \right), \end{aligned} \quad (42)$$

with the 3×3 matrixes $\underline{\mathbf{a}}^\#$ and $\underline{\check{\rho}}^\#$ having entries

$$\left. \begin{aligned} \left[\underline{\mathbf{a}}^\# \right]_{pq} &= \left[\underline{\mathbf{a}}(\hat{\mathbf{k}}) \right]_{pq} \\ \left[\underline{\check{\rho}}^\# \right]_{pq} &= \left[\underline{\check{\rho}}^{(ocm)} \right]_{pq} \end{aligned} \right\}, \quad (p, q = 1, 2, 3). \quad (43)$$

Through exploiting eqs. (38) and (40), the integrals in eqs. (33) and (34) with respect to k can be evaluated by means of calculus of residues: The roots of $\Delta(\mathbf{k}) = 0$ give rise to seven poles in the complex- k plane, located at $k = 0, \pm p_1, \pm p_2, \pm p_3$, which are chosen such that p_n ($n = 1, 2, 3$) lie in the upper half of the complex plane. From eq. (42), we find that the nonzero poles satisfy

$$p_1^2 = P_A - \frac{1}{3} \left(\frac{2^{1/3} P_B}{P_C} - \frac{P_C}{2^{1/3}} \right), \quad (44)$$

$$p_2^2 = P_A + \frac{1}{3} \left(\frac{(1+i\sqrt{3})P_B}{2^{2/3}P_C} - \frac{(1-i\sqrt{3})P_C}{2^{4/3}} \right), \quad (45)$$

$$p_3^2 = P_A + \frac{1}{3} \left(\frac{(1-i\sqrt{3})P_B}{2^{2/3}P_C} - \frac{(1+i\sqrt{3})P_C}{2^{4/3}} \right), \quad (46)$$

wherein

$$P_A = \frac{\omega^2 \text{tr} \left\{ \text{adj} \left[\underline{\underline{\mathbf{a}}}(\hat{\mathbf{k}}) \right] \cdot \underline{\underline{\rho}}^{(ocm)} \right\}}{3 \det \left[\underline{\underline{\mathbf{a}}}(\hat{\mathbf{k}}) \right]}, \quad (47)$$

$$P_B = -C_A^2 + 3C_B, \quad (48)$$

$$P_C = \left[P_D + (4P_B^3 + P_D^2)^{1/2} \right]^{1/3}, \quad (49)$$

$$P_D = -2C_A^3 + 9C_A C_B - 27C_C, \quad (50)$$

with

$$C_A = \frac{-\omega^2 \text{tr} \left\{ \text{adj} \left[\underline{\underline{\mathbf{a}}}(\hat{\mathbf{k}}) \right] \cdot \underline{\underline{\rho}}^{(ocm)} \right\}}{\det \left[\underline{\underline{\mathbf{a}}}(\hat{\mathbf{k}}) \right]}, \quad (51)$$

$$C_B = \frac{\omega^4}{\det \left[\underline{\underline{\mathbf{a}}}(\hat{\mathbf{k}}) \right]} \left\{ \left[\underline{\underline{\mathbf{a}}}(\hat{\mathbf{k}}) \right]_{44} \text{tr} \left[\underline{\underline{\mathbf{a}}}^\#(\hat{\mathbf{k}}) \cdot \text{adj} \left(\underline{\underline{\rho}}^\# \right) \right] + \left[\underline{\underline{\mathbf{a}}}(\hat{\mathbf{k}}) \right]_{41} \left[\underline{\underline{\mathbf{a}}}(\hat{\mathbf{k}}) \right]_{14} \left[\text{adj} \left(\underline{\underline{\rho}}^{(ocm)} \right) \right]_{11} \right. \\ \left. + \left[\underline{\underline{\mathbf{a}}}(\hat{\mathbf{k}}) \right]_{42} \left[\underline{\underline{\mathbf{a}}}(\hat{\mathbf{k}}) \right]_{24} \left[\text{adj} \left(\underline{\underline{\rho}}^{(ocm)} \right) \right]_{22} + \left[\underline{\underline{\mathbf{a}}}(\hat{\mathbf{k}}) \right]_{43} \left[\underline{\underline{\mathbf{a}}}(\hat{\mathbf{k}}) \right]_{34} \left[\text{adj} \left(\underline{\underline{\rho}}^{(ocm)} \right) \right]_{33} \right\}, \quad (52)$$

$$C_C = \frac{-\omega^6 \text{tr} \left\{ \text{adj} \left[\underline{\underline{\rho}}^{(ocm)} \right] \cdot \underline{\underline{\mathbf{a}}}(\hat{\mathbf{k}}) \right\}}{\det \left[\underline{\underline{\mathbf{a}}}(\hat{\mathbf{k}}) \right]}. \quad (53)$$

Thus, by application of the Cauchy residue theorem [29], the SPFT estimates are delivered in terms of two-dimensional integrals as

$$\check{C}_{lMPq}^{(spft)} = \check{C}_{lMPq}^{(ocm)} + \frac{\omega^2 f^{(1)} f^{(2)}}{4\pi i} \int_{\phi=0}^{2\pi} \int_{\theta=0}^{\pi} d\phi d\theta \frac{k_t \sin \theta}{(k\sigma)^2 \det \left[\underline{\underline{\mathbf{a}}}(\hat{\mathbf{k}}) \right]} \left[\underline{\underline{\rho}}^{(ocm)} \right]_{XY} \left[\underline{\underline{\mathbf{b}}}(\hat{\mathbf{k}}) \right]_{YU} \\ \times \left(\left\{ \xi_{lMr s}^{(2)} - \xi_{lMr s}^{(1)} \right\} \left\{ k_s \left[\underline{\underline{\mathbf{a}}}^{-1}(\hat{\mathbf{k}}) \right]_{rX} + k_r \left[\underline{\underline{\mathbf{a}}}^{-1}(\hat{\mathbf{k}}) \right]_{sX} \right\} \right. \\ \left. + \left\{ \xi_{lm4s}^{(2)} - \xi_{lm4s}^{(1)} \right\} \left\{ k_s \left[\underline{\underline{\mathbf{a}}}^{-1}(\hat{\mathbf{k}}) \right]_{4X} \right\} \right) \left(\xi_{tUPq}^{(2)} - \xi_{tUPq}^{(1)} \right) \quad (54)$$

and

$$\check{\rho}_{MP}^{(spft)} = \check{\rho}_{MP}^{(ocm)} - \frac{\omega^2 f^{(1)} f^{(2)} \left(\check{\rho}_{MS}^{(2)} - \check{\rho}_{MS}^{(1)} \right) \left(\check{\rho}_{UP}^{(2)} - \check{\rho}_{UP}^{(1)} \right)}{2\pi i} \int_{\phi=0}^{2\pi} \int_{\theta=0}^{\pi} d\phi d\theta \frac{\sin \theta}{\det \left[\underline{\underline{\mathbf{a}}}(\hat{\mathbf{k}}) \right]} \left[\underline{\underline{\mathbf{b}}}(\hat{\mathbf{k}}) \right]_{SU}, \quad (55)$$

where the 4×4 matrix

$$\begin{aligned} \underline{\mathbf{b}}(\hat{\mathbf{k}}) = & \frac{1}{2i} \left\{ \frac{e^{iL\sigma p_1} \underline{\mathbf{D}}(p_1 \underline{\mathbf{U}} \cdot \hat{\mathbf{k}})}{\sigma p_1^4 (p_1^2 - p_2^2)(p_1^2 - p_3^2)} \left(1 - iL\sigma p_1\right) - \frac{e^{iL\sigma p_2} \underline{\mathbf{D}}(p_2 \underline{\mathbf{U}} \cdot \hat{\mathbf{k}})}{\sigma p_2^4 (p_1^2 - p_2^2)(p_2^2 - p_3^2)} \left(1 - iL\sigma p_2\right) \right. \\ & + \frac{e^{iL\sigma p_3} \underline{\mathbf{D}}(p_3 \underline{\mathbf{U}} \cdot \hat{\mathbf{k}})}{\sigma p_3^4 (p_2^2 - p_3^2)(p_1^2 - p_3^2)} \left(1 - iL\sigma p_3\right) \\ & \left. - \frac{1}{\sigma p_1^2 p_2^2 p_3^2} \left[\underline{\mathbf{D}}(\mathbf{0}) \left(\frac{1}{p_1^2} + \frac{1}{p_2^2} + \frac{1}{p_3^2} + \frac{\sigma^2 L^2}{2} \right) + \frac{1}{2} \frac{\partial^2}{\partial k^2} \underline{\mathbf{D}}(\mathbf{0}) \right] \right\}. \end{aligned} \quad (56)$$

The expressions for the second-order SPFT estimates $\check{C}_{lMPq}^{(spft)}$ and $\check{\rho}_{MP}^{(spft)}$ in eqs. (54) and (55) may be evaluated by standard numerical methods [30].

It is particularly noteworthy that $\check{C}_{lMPq}^{(spft)}$ and $\check{\rho}_{MP}^{(spft)}$ are complex-valued for $L > 0$, even when the corresponding quantities for the component materials, i.e., $\check{C}_{lMPq}^{(\ell)}$ and $\check{\rho}_{MP}^{(\ell)}$ ($\ell = 1, 2$), are real-valued. This reflects the fact that the SPFT accommodates losses due to scattering [17]. From energy considerations, the imaginary part of the extended compliance matrix, namely [22]

$$\underline{\mathbf{M}}^{(spft)} = \begin{pmatrix} \left(\underline{\mathbf{C}}^{(spft)} \right)^{-1} & \left(\underline{\mathbf{C}}^{(spft)} \right)^{-1} \cdot \underline{\mathbf{e}}^{(spft)} \\ \left[\left(\underline{\mathbf{C}}^{(spft)} \right)^{-1} \cdot \underline{\mathbf{e}}^{(spft)} \right]^T & \underline{\mathbf{e}}^{(spft)} + \left(\underline{\mathbf{e}}^{(spft)} \right)^T \cdot \left(\underline{\mathbf{C}}^{(spft)} \right)^{-1} \cdot \underline{\mathbf{e}}^{(spft)} \end{pmatrix}, \quad (57)$$

is required to be positive definite for passive materials [31]. The constitutive matrixes $\underline{\mathbf{C}}^{(spft)}$, $\underline{\mathbf{e}}^{(spft)}$ and $\underline{\mathbf{e}}^{(spft)}$ on the right side of eq. (57) are related to the extended stiffness matrix $\check{\underline{\mathbf{C}}}^{(spft)}$ (and thereby to the extended stiffness symbol $\check{C}_{lMPq}^{(spft)}$) per eq. (7).

3 Numerical results

3.1 Preliminaries

In order to illustrate the theory presented in §2, let us now consider a representative numerical example. A comparison for the SPFT estimate of the HCM constitutive parameters is provided by the corresponding results computed using the Mori–Tanaka formalism [9, 12, 23, 24]. In the case of orthorhombic $mm2$ piezoelectric component materials, the Mori–Tanaka estimate of the extended stiffness matrix for the HCM is given by [13]

$$\check{\underline{\mathbf{C}}}^{(MT)} = \check{\underline{\mathbf{C}}}^{(1)} + f^{(2)} \left(\check{\underline{\mathbf{C}}}^{(2)} - \check{\underline{\mathbf{C}}}^{(1)} \right) \cdot \underline{\mathbf{B}}^{(MT)} \cdot \left[f^{(1)} \underline{\boldsymbol{\tau}} + f^{(2)} \underline{\mathbf{B}}^{(MT)} \right]^\dagger, \quad (58)$$

where the 12×12 matrix

$$\underline{\mathbf{B}}^{(MT)} = \left[\underline{\boldsymbol{\tau}} + \underline{\mathbf{S}}^{(Esh)} \cdot \left(\check{\underline{\mathbf{C}}}^{(1)} \right)^\dagger \cdot \left(\check{\underline{\mathbf{C}}}^{(2)} - \check{\underline{\mathbf{C}}}^{(1)} \right) \right]^\dagger, \quad (59)$$

with $\underline{\mathbf{S}}^{(Esh)}$ being the 12×12 matrix representation of the Eshelby tensor [7, 10, 32]. Details on evaluating $\underline{\mathbf{S}}^{(Esh)}$ can be found in Appendix B.

In the following, we present the numerical evaluation of the 12×12 extended stiffness matrix of the HCM, namely $\check{\underline{\mathbf{C}}}^{(hcm)}$, as estimated by the lowest-order SPFT (i.e., $hcm = ocm$), the second-order SPFT (i.e., $hcm = spft$) and the Mori–Tanaka formalism (i.e., $hcm = MT$). The matrix $\check{\underline{\mathbf{C}}}^{(hcm)}$ has the form represented in eq. (7). The second-order SPFT density tensor $\rho_{MP}^{(spft)}$ is also evaluated; the numerical evaluation of the lowest-order SPFT density $\rho_{MP}^{(ocm)}$ need not be presented here as this quantity is simply the volume average

of the densities of the component materials. An angular frequency of $\omega = 2\pi \times 10^6 \text{ s}^{-1}$ was selected for all second-order SPFT computations.

The eccentricities of the ellipsoidal component particles are specified by the shape parameters $\{a, b, c\}$, per eqs. (14) and (15). To allow direct comparison with results from previous studies [13], component material ‘1’ was taken to be the piezoelectric material polyvinylidene fluoride (PVDF) while component material ‘2’ was taken to be the thermoplastic polyimide LaRC-SI, which has no piezoelectric properties. The stiffness constitutive parameters of the component materials are tabulated in Table 1. The nonzero piezoelectric constitutive parameters of PVDF are: $e_{113} \equiv e_{31} = 0.024$, $e_{223} \equiv e_{32} = 0.001$ and $e_{333} \equiv e_{33} = -0.027$ in units of C m^{-2} . The dielectric constitutive parameters of PVDF are: $\epsilon_{11} = 7.4$, $\epsilon_{22} = 9.6$ and $\epsilon_{33} = 7.6$, whereas those of LaRC-SI are: $\epsilon_{11} = \epsilon_{22} = \epsilon_{33} = 2.8$, all in units of $\epsilon_0 = 8.854 \times 10^{-12} \text{ F m}^{-1}$ (the permittivity of free space). Lastly, the densities of PVDF and LaRC-SI are 1750 and 1376, respectively, in units of kg m^{-3} .

Stiffness parameter	PVDF (GPa)	LaRC-SI (GPa)
$C_{1111} \equiv C_{11}$	3.8	8.1
$C_{1122} \equiv C_{12}$	1.9	5.4
$C_{1133} \equiv C_{13}$	1.0	5.4
$C_{2222} \equiv C_{22}$	3.2	8.1
$C_{2233} \equiv C_{23}$	0.9	5.4
$C_{3333} \equiv C_{33}$	1.2	8.1
$C_{2323} \equiv C_{44}$	0.7	1.4
$C_{1313} \equiv C_{55}$	0.9	1.4
$C_{1212} \equiv C_{66}$	0.9	1.4

Table 1: The stiffness constitutive parameters of the component materials in units of GPa (after [13]).

3.2 Lowest-order SPFT

We begin by considering the lowest-order SPFT estimates of the HCM constitutive parameters. In Fig. 1, components of the HCM extended stiffness matrix $\underline{\underline{\check{C}}}^{\check{y}(hcm)}$, as computed using the lowest-order SPFT and the Mori–Tanaka formalism, are plotted as functions of volume fraction $f^{(2)}$ for the case where the component particles are spherical (i.e., $a = b = c$). Plots of only a representative selection of the components of $\underline{\underline{\check{C}}}^{\check{y}(hcm)}$ are presented in Fig. 1; plots for those components which are not presented in Fig. 1 are qualitatively similar to those that are presented. Only relatively minor differences between the lowest-order SPFT estimates and the Mori–Tanaka estimates are observed, with the differences between the two being greatest for mid-range values of $f^{(2)}$. Plots for both the SPFT and Mori–Tanaka estimates are necessarily constrained by the limits

$$\lim_{f^{(2)} \rightarrow 0} \underline{\underline{\check{C}}}^{\check{y}(hcm)} = \underline{\underline{\check{C}}}^{\check{y}(1)}, \quad \lim_{f^{(2)} \rightarrow 1} \underline{\underline{\check{C}}}^{\check{y}(hcm)} = \underline{\underline{\check{C}}}^{\check{y}(2)}. \quad (60)$$

The corresponding graphs for the cases where the components particles are described by the shape parameters $\{a/c = 5, b/c = 1.5\}$ and $\{a/c = 10, b/c = 2\}$ are provided in Figs. 2 and 3, respectively. A comparison of Figs. 1–3 reveals that the differences between the lowest-order SPFT and Mori–Tanaka estimates are accentuated as the component particles become more eccentric in shape, especially at mid-range values of $f^{(2)}$ for the piezoelectric parameters and the dielectric parameters.

3.3 Second-order SPFT estimate

Now let us turn to the second-order SPFT estimates of the HCM constitutive parameters. We considered these quantities as functions of $\bar{k}L$, where \bar{k} is an approximate upper bound on the wavenumbers supported

by the HCM, as estimated by [20]

$$\bar{k} = \frac{\omega}{2} \left(\sqrt{\frac{\bar{\rho}}{\lambda + 2\bar{\mu}}} + \sqrt{\frac{\bar{\rho}}{\bar{\mu}}} \right), \quad (61)$$

wherein

$$\left. \begin{aligned} \bar{\lambda} &= \frac{1}{6} \sum_{\ell=1}^2 \left(\left| \left[\underline{\underline{\mathbf{C}}}^{(\ell)} \right]_{12} \right| + \left| \left[\underline{\underline{\mathbf{C}}}^{(\ell)} \right]_{13} \right| + \left| \left[\underline{\underline{\mathbf{C}}}^{(\ell)} \right]_{23} \right| \right) \\ \bar{\mu} &= \frac{1}{6} \sum_{\ell=1}^2 \left(\left| \left[\underline{\underline{\mathbf{C}}}^{(\ell)} \right]_{44} \right| + \left| \left[\underline{\underline{\mathbf{C}}}^{(\ell)} \right]_{55} \right| + \left| \left[\underline{\underline{\mathbf{C}}}^{(\ell)} \right]_{66} \right| \right) \\ \bar{\rho} &= \frac{1}{2} \sum_{\ell=1}^2 \rho^{(\ell)} \end{aligned} \right\}; \quad (62)$$

and L is the correlation length associated with the two-point covariance function (18). In Fig. 4, the real and imaginary parts of the components of $\tilde{\underline{\underline{\mathbf{C}}}}^{(spf)} = \check{\underline{\underline{\mathbf{C}}}}^{(spf)} - \check{\underline{\underline{\mathbf{C}}}}^{(ocm)}$ are plotted against $\bar{k}L$ for $f^{(2)} = 0.5$. The values of the shape parameters $\{a, b, c\}$ correspond to those used in the calculations for Figs. 1–3. As in §3.2, only a representative selection of the components of $\tilde{\underline{\underline{\mathbf{C}}}}^{(spf)}$ are plotted in Fig. 4; the graphs for those components that are not represented in Fig. 4 are qualitatively similar to the graphs which do appear.

The second-order corrections to the lowest-order SPFT estimates are observed in Fig. 4 to grow exponentially in magnitude as the correlation length increases from zero. Furthermore, the magnitudes of both the real and imaginary parts of $\check{\underline{\underline{\mathbf{C}}}}^{(spf)}$ generally grow faster with increasing correlation length when the component particles are more eccentric in shape. At $L = 0$, the second-order and lowest-order SPFT estimates coincide. While the second-order corrections are relatively small compared to the lowest-order SPFT estimates, a highly significant feature of the second-order corrections is that these are complex-valued with nonzero imaginary parts, even though $\check{\underline{\underline{\mathbf{C}}}}^{(a,b)}$ and $\check{\underline{\underline{\mathbf{C}}}}^{(ocm)}$ are purely real-valued. We note that for all computations the imaginary part of the extended compliance matrix $\check{\underline{\underline{\mathbf{M}}}}^{(spf)}$ was found to be positive definite, which corresponds to positive loss [31]. Thus, the emergence of nonzero imaginary parts of $\check{\underline{\underline{\mathbf{C}}}}^{(spf)}$ indicates that the HCM has acquired a dissipative nature, despite the component materials being nondissipative. The dissipation is attributed to scattering losses, since the second-order SPFT takes into account interactions between spatially-distinct scattering particles via the two-point covariance function (18). As the correlation length increases, the number of scattering particles that can mutually interact also increases, thereby increasing the scattering loss per unit volume.

Finally, we turn to the second-order SPFT estimate of the HCM density. The real and imaginary parts of the matrix entry $\left[\tilde{\underline{\underline{\rho}}}^{(spf)} \right]_{11}$, wherein $\tilde{\underline{\underline{\rho}}}^{(spf)} = \check{\underline{\underline{\rho}}}^{(spf)} - \check{\underline{\underline{\rho}}}^{(ocm)}$, are plotted as functions of $\bar{k}L$ in Fig. 5. The corresponding graphs for $\left[\tilde{\underline{\underline{\rho}}}^{(spf)} \right]_{22}$ and $\left[\tilde{\underline{\underline{\rho}}}^{(spf)} \right]_{33}$ are much the same as those for $\left[\tilde{\underline{\underline{\rho}}}^{(spf)} \right]_{11}$ but with minor differences in magnitudes. The second-order SPFT estimates of the HCM density exhibit characteristics similar to those of the corresponding HCM stiffness, piezoelectric and dielectric constitutive parameters. That is, $\lim_{L \rightarrow 0} \rho_{aa}^{(spf)} = \rho^{(ocm)}$ and $\left| \check{\rho}_{aa}^{(spf)} \right| \ll \left| \rho^{(ocm)} \right|$ for $a = 1, 2$ and 3. Also, the differences between $\check{\underline{\underline{\rho}}}^{(spf)}$ and $\check{\underline{\underline{\rho}}}^{(ocm)}$ increase exponentially as the correlation length increases, and this effect is most accentuated when the component particles are most eccentric in shape.

We remark that a complex-valued, anisotropic density also crops up in the second-order elastodynamic SPFT for orthotropic HCMs [20], as well as in other homogenization scenarios [33, 34].

4 Closing remarks

The linear SPFT has been fully developed for the case of orthorhombic $mm2$ piezoelectric HCMs, based on component materials distributed as oriented ellipsoidal particles. The multifunctionality of such HCMs is

central to the notion of metamaterials [5]. The second-order estimates of the HCM constitutive parameters are expressed in terms of numerically-tractable two-dimensional integrals, for a specific choice of two-point covariance function. This theoretical result further extends the application of the SPFT in the homogenization of complex composites, effectively bridging the elastodynamic SPFT for orthotropic HCMs [19, 20] and the electromagnetic SPFT for anisotropic dielectric HCMs [35, 36]. Furthermore, the path has now been cleared towards the development of the SPFT for piezoelectric/piezomagnetic HCMs [37], with bianisotropic electromagnetic properties [17]. Let us remark that the mathematical description of piezoelectric HCMs presented herein also extends to electrokinetic processes [38].

From our theoretical considerations and representative numerical studies, the following conclusions were drawn:

- The lowest-order SPFT estimate of the stiffness, piezoelectric and dielectric properties of the HCM are qualitatively similar to those estimates provided by the Mori-Tanaka formalism.
- Differences between the estimates of the lowest-order SPFT and the Mori-Tanaka formalism are greatest at mid-range values of the volume fraction, and accentuated when the component particles are eccentric in shape.
- The second-order SPFT provides a correction to the lowest-order estimate of the HCM constitutive properties. The magnitude of this correction is generally larger when the component particles are more eccentric in shape, and vanishes as the correlation length tends to zero.
- While the correction provided by the second-order SPFT is relatively small in magnitude, it is highly significant as it indicates dissipation due to scattering loss.

Appendix A

The extended symbol \check{A}_{aMPq} ($a, q \in \{1, 2, 3\}$, $M, P \in \{1, 2, 3, 4\}$) may be conveniently represented by the 12×12 matrix with entries $\left[\check{\underline{\underline{A}}} \right]_{\gamma\kappa}$ ($\gamma, \kappa \in [1, 12]$), upon replacing the index pair aM with γ and the index pair Pq with κ . For the most general 12×12 matrix encountered in this paper, which has the form

$$\check{\underline{\underline{A}}} = \begin{pmatrix} A_{1,1} & A_{1,2} & A_{1,3} & 0 & 0 & 0 & 0 & 0 & 0 & 0 & 0 & 0 & A_{1,12} \\ A_{2,1} & A_{2,2} & A_{2,3} & 0 & 0 & 0 & 0 & 0 & 0 & 0 & 0 & 0 & A_{2,12} \\ A_{3,1} & A_{3,2} & A_{3,3} & 0 & 0 & 0 & 0 & 0 & 0 & 0 & 0 & 0 & A_{3,12} \\ 0 & 0 & 0 & A_{4,4} & 0 & 0 & A_{4,4} & 0 & 0 & 0 & A_{4,11} & 0 & 0 \\ 0 & 0 & 0 & 0 & A_{5,5} & 0 & 0 & A_{5,5} & 0 & A_{5,10} & 0 & 0 & 0 \\ 0 & 0 & 0 & 0 & 0 & A_{6,6} & 0 & 0 & A_{6,6} & 0 & 0 & 0 & 0 \\ 0 & 0 & 0 & A_{4,4} & 0 & 0 & A_{4,4} & 0 & 0 & 0 & A_{4,11} & 0 & 0 \\ 0 & 0 & 0 & 0 & A_{5,5} & 0 & 0 & A_{5,5} & 0 & A_{5,10} & 0 & 0 & 0 \\ 0 & 0 & 0 & 0 & 0 & A_{6,6} & 0 & 0 & A_{6,6} & 0 & 0 & 0 & 0 \\ 0 & 0 & 0 & 0 & A_{10,5} & 0 & 0 & A_{10,5} & 0 & A_{10,10} & 0 & 0 & 0 \\ 0 & 0 & 0 & A_{11,4} & 0 & 0 & A_{11,4} & 0 & 0 & 0 & A_{11,11} & 0 & 0 \\ A_{12,1} & A_{12,2} & A_{12,3} & 0 & 0 & 0 & 0 & 0 & 0 & 0 & 0 & 0 & A_{12,12} \end{pmatrix}, \quad (63)$$

the correspondence between the extended symbol indexes and the matrix indexes is provided in Table 2. The scheme presented in Table 2 also relates the extended symbol \check{t}_{aM} to the corresponding column 12-vector entries $\left[\check{\underline{\underline{t}}} \right]_{\gamma}$.

We introduce the matrix $\check{\underline{\underline{A}}}^{\dagger}$ which plays a role similar to the matrix inverse insofar as

$$\check{\underline{\underline{A}}}^{\dagger} \cdot \check{\underline{\underline{A}}} = \check{\underline{\underline{A}}} \cdot \check{\underline{\underline{A}}}^{\dagger} = \underline{\underline{\tau}}. \quad (64)$$

aM or Pq	γ or κ	aM or Pq	γ or κ	aM or Pq	γ or κ	aM or Pq	γ or κ
11	1	23 or 32	4	23 or 32	7	14 or 41	10
22	2	13 or 31	5	13 or 31	8	24 or 42	11
33	3	12 or 21	6	12 or 21	9	34 or 43	12

Table 2: Conversion between extended symbol and matrix notation.

Herein,

$$\underline{\underline{\tau}} = \begin{pmatrix} \underline{\underline{\mathbf{I}}} & \underline{\underline{\mathbf{0}}}_{3 \times 3} & \underline{\underline{\mathbf{0}}}_{3 \times 3} & \underline{\underline{\mathbf{0}}}_{3 \times 3} \\ \underline{\underline{\mathbf{0}}}_{3 \times 3} & \frac{1}{2}\underline{\underline{\mathbf{I}}} & \frac{1}{2}\underline{\underline{\mathbf{I}}} & \underline{\underline{\mathbf{0}}}_{3 \times 3} \\ \underline{\underline{\mathbf{0}}}_{3 \times 3} & \frac{1}{2}\underline{\underline{\mathbf{I}}} & \frac{1}{2}\underline{\underline{\mathbf{I}}} & \underline{\underline{\mathbf{0}}}_{3 \times 3} \\ \underline{\underline{\mathbf{0}}}_{3 \times 3} & \underline{\underline{\mathbf{0}}}_{3 \times 3} & \underline{\underline{\mathbf{0}}}_{3 \times 3} & \underline{\underline{\mathbf{I}}} \end{pmatrix} \quad (65)$$

is the 12×12 matrix representation of the extended identity symbol, with $\underline{\underline{\mathbf{I}}}$ being the 3×3 identity matrix, and we have

$$\underline{\underline{\mathbf{A}}} \cdot \underline{\underline{\tau}} = \underline{\underline{\tau}} \cdot \underline{\underline{\mathbf{A}}} = \underline{\underline{\mathbf{A}}}. \quad (66)$$

The matrix $\underline{\underline{\mathbf{A}}}^\dagger$ has the form

$$\underline{\underline{\mathbf{A}}}^\dagger = \begin{pmatrix} \dagger_{1,1} & \dagger_{1,2} & \dagger_{1,3} & 0 & 0 & 0 & 0 & 0 & 0 & 0 & 0 & \dagger_{1,12} \\ \dagger_{2,1} & \dagger_{2,2} & \dagger_{2,3} & 0 & 0 & 0 & 0 & 0 & 0 & 0 & 0 & \dagger_{2,12} \\ \dagger_{3,1} & \dagger_{3,2} & \dagger_{3,3} & 0 & 0 & 0 & 0 & 0 & 0 & 0 & 0 & \dagger_{3,12} \\ 0 & 0 & 0 & \frac{\dagger_{4,4}}{2} & 0 & 0 & \frac{\dagger_{4,4}}{2} & 0 & 0 & 0 & \dagger_{4,11} & 0 \\ 0 & 0 & 0 & 0 & \frac{\dagger_{5,5}}{2} & 0 & 0 & \frac{\dagger_{5,5}}{2} & 0 & \dagger_{5,10} & 0 & 0 \\ 0 & 0 & 0 & 0 & 0 & \frac{\dagger_{6,6}}{2} & 0 & 0 & \frac{\dagger_{6,6}}{2} & 0 & 0 & 0 \\ 0 & 0 & 0 & \frac{\dagger_{4,4}}{2} & 0 & 0 & \frac{\dagger_{4,4}}{2} & 0 & 0 & 0 & \dagger_{4,11} & 0 \\ 0 & 0 & 0 & 0 & \frac{\dagger_{5,5}}{2} & 0 & 0 & \frac{\dagger_{5,5}}{2} & 0 & \dagger_{5,10} & 0 & 0 \\ 0 & 0 & 0 & 0 & 0 & \frac{\dagger_{6,6}}{2} & 0 & 0 & \frac{\dagger_{6,6}}{2} & 0 & 0 & 0 \\ 0 & 0 & 0 & 0 & \dagger_{10,5} & 0 & 0 & \dagger_{10,5} & 0 & \dagger_{10,10} & 0 & 0 \\ 0 & 0 & 0 & \dagger_{11,4} & 0 & 0 & \dagger_{11,4} & 0 & 0 & 0 & \dagger_{11,11} & 0 \\ \dagger_{12,1} & \dagger_{12,2} & \dagger_{12,3} & 0 & 0 & 0 & 0 & 0 & 0 & 0 & 0 & \dagger_{12,12} \end{pmatrix}, \quad (67)$$

with entries

$$\dagger_{1,1} = (-A_{12,3}A_{2,2}A_{3,12} + A_{12,2}A_{2,3}A_{3,12} + A_{12,3}A_{2,12}A_{3,2} - A_{12,12}A_{2,3}A_{3,2} - A_{12,2}A_{2,12}A_{3,3} + A_{12,12}A_{2,2}A_{3,3})/\Lambda, \quad (68)$$

$$\dagger_{1,2} = (A_{1,2}A_{12,3}A_{3,12} - A_{12,2}A_{1,3}A_{3,12} - A_{1,12}A_{12,3}A_{3,2} + A_{12,12}A_{1,3}A_{3,2} - A_{1,2}A_{12,12}A_{3,3} + A_{1,12}A_{12,2}A_{3,3})/\Lambda, \quad (69)$$

$$\dagger_{1,3} = (-A_{1,2}A_{12,3}A_{2,12} + A_{12,2}A_{1,3}A_{2,12} + A_{1,12}A_{12,3}A_{2,2} - A_{12,12}A_{1,3}A_{2,2} + A_{1,2}A_{12,12}A_{2,3} - A_{1,12}A_{12,2}A_{2,3})/\Lambda, \quad (70)$$

$$\dagger_{2,1} = (-A_{12,3}A_{2,12}A_{3,1} + A_{12,12}A_{2,3}A_{3,1} + A_{12,3}A_{2,1}A_{3,12} - A_{12,1}A_{2,3}A_{3,12} - A_{12,12}A_{2,1}A_{3,3} + A_{12,1}A_{2,12}A_{3,3})/\Lambda, \quad (71)$$

$$\dagger_{2,2} = (A_{1,12}A_{12,3}A_{3,1} - A_{12,12}A_{1,3}A_{3,1} - A_{1,1}A_{12,3}A_{3,12} + A_{12,1}A_{1,3}A_{3,12} - A_{1,12}A_{12,1}A_{3,3} + A_{1,1}A_{12,12}A_{3,3})/\Lambda, \quad (72)$$

$$\dagger_{2,3} = (-A_{1,12}A_{12,3}A_{2,1} + A_{12,12}A_{1,3}A_{2,1} + A_{1,1}A_{12,3}A_{2,12} - A_{12,1}A_{1,3}A_{2,12} + A_{1,12}A_{12,1}A_{2,3} - A_{1,1}A_{12,12}A_{2,3})/\Lambda, \quad (73)$$

$$\dagger_{3,1} = (A_{12,2}A_{2,12}A_{3,1} - A_{12,12}A_{2,2}A_{3,1} - A_{12,2}A_{2,1}A_{3,12} + A_{12,1}A_{2,2}A_{3,12} + A_{12,12}A_{2,1}A_{3,2} - A_{12,1}A_{2,12}A_{3,2})/\Lambda, \quad (74)$$

$$\dagger_{3,2} = (A_{1,2}A_{12,12}A_{3,1} - A_{1,12}A_{12,2}A_{3,1} - A_{1,2}A_{12,1}A_{3,12} + A_{1,1}A_{12,2}A_{3,12} + A_{1,12}A_{12,1}A_{3,2} - A_{1,1}A_{12,12}A_{3,2})/\Lambda, \quad (75)$$

$$\dagger_{3,3} = (-A_{1,2}A_{12,12}A_{2,1} + A_{1,12}A_{12,2}A_{2,1} + A_{1,2}A_{12,1}A_{2,12} - A_{1,1}A_{12,2}A_{2,12} - A_{1,12}A_{12,1}A_{2,2} + A_{1,1}A_{12,12}A_{2,2})/\Lambda, \quad (76)$$

$$\dagger_{4,4} = \frac{A_{11,11}}{2(A_{11,11}A_{4,4} - A_{4,11}A_{11,4})}, \quad (77)$$

$$\dagger_{5,5} = \frac{A_{10,10}}{2(A_{10,10}A_{5,5} - A_{5,10}A_{10,5})}, \quad (78)$$

$$\dagger_{6,6} = \frac{1}{2A_{6,6}}, \quad (79)$$

$$\dagger_{10,10} = \frac{A_{5,5}}{(A_{10,10}A_{5,5} - A_{10,5}A_{5,10})}, \quad (80)$$

$$\dagger_{11,11} = \frac{A_{4,4}}{(A_{11,11}A_{4,4} - A_{11,4}A_{4,11})}, \quad (81)$$

$$\dagger_{12,12} = (-A_{1,3}A_{2,2}A_{3,1} + A_{1,2}A_{2,3}A_{3,1} + A_{1,3}A_{2,1}A_{3,2} - A_{1,1}A_{2,3}A_{3,2} - A_{1,2}A_{2,1}A_{3,3} + A_{1,1}A_{2,2}A_{3,3})/\Lambda, \quad (82)$$

$$\dagger_{1,12} = (A_{1,3}A_{2,2}A_{3,12} - A_{1,2}A_{2,3}A_{3,12} - A_{1,3}A_{2,12}A_{3,2} + A_{1,12}A_{2,3}A_{3,2} + A_{1,2}A_{2,12}A_{3,3} - A_{1,12}A_{2,2}A_{3,3})/\Lambda, \quad (83)$$

$$\dagger_{2,12} = (A_{1,3}A_{2,12}A_{3,1} - A_{1,12}A_{2,3}A_{3,1} - A_{1,3}A_{2,1}A_{3,12} + A_{1,1}A_{2,3}A_{3,12} + A_{1,12}A_{2,1}A_{3,3} - A_{1,1}A_{2,12}A_{3,3})/\Lambda, \quad (84)$$

$$\dagger_{3,12} = (-A_{1,2}A_{2,12}A_{3,1} + A_{1,12}A_{2,2}A_{3,1} + A_{1,2}A_{2,1}A_{3,12} - A_{1,1}A_{2,2}A_{3,12} - A_{1,12}A_{2,1}A_{3,2} + A_{1,1}A_{2,12}A_{3,2})/\Lambda, \quad (85)$$

$$\dagger_{4,11} = \frac{A_{4,11}}{2(A_{11,4}A_{4,11} - A_{11,11}A_{4,4})}, \quad (86)$$

$$\dagger_{5,10} = \frac{A_{5,10}}{2(A_{5,10}A_{10,5} - A_{10,10}A_{5,5})}, \quad (87)$$

$$\dagger_{12,1} = (A_{12,3}A_{2,2}A_{3,1} - A_{12,2}A_{2,3}A_{3,1} - A_{12,3}A_{2,1}A_{3,2} + A_{12,1}A_{2,3}A_{3,2} + A_{12,2}A_{2,1}A_{3,3} - A_{12,1}A_{2,2}A_{3,3})/\Lambda, \quad (88)$$

$$\dagger_{12,2} = (-A_{1,2}A_{12,3}A_{3,1} + A_{12,2}A_{1,3}A_{3,1} + A_{1,1}A_{12,3}A_{3,2} - A_{12,1}A_{1,3}A_{3,2} + A_{1,2}A_{12,1}A_{3,3} - A_{1,1}A_{12,2}A_{3,3})/\Lambda, \quad (89)$$

$$\dagger_{12,3} = (A_{1,2}A_{12,3}A_{2,1} - A_{12,2}A_{1,3}A_{2,1} - A_{1,1}A_{12,3}A_{2,2} + A_{12,1}A_{1,3}A_{2,2} - A_{1,2}A_{12,1}A_{2,3} + A_{1,1}A_{12,2}A_{2,3})/\Lambda, \quad (90)$$

$$\dagger_{11,4} = \frac{A_{11,4}}{2(A_{11,4}A_{4,11} - A_{11,11}A_{4,4})}, \quad (91)$$

$$\dagger_{10,5} = \frac{A_{10,5}}{2(A_{10,5}A_{5,10} - A_{10,10}A_{5,5})}, \quad (92)$$

$$(93)$$

where the scalar

$$\begin{aligned} \Lambda = & A_{1,12}A_{12,3}A_{2,2}A_{3,1} - A_{12,12}A_{1,3}A_{2,2}A_{3,1} - A_{1,1}A_{12,3}A_{2,2}A_{3,12} + A_{12,1}A_{1,3}A_{2,2}A_{3,12} - \\ & A_{1,12}A_{12,3}A_{2,1}A_{3,2} + A_{12,12}A_{1,3}A_{2,1}A_{3,2} + A_{1,1}A_{12,3}A_{2,12}A_{3,2} - A_{12,1}A_{1,3}A_{2,12}A_{3,2} + \\ & A_{1,12}A_{12,1}A_{2,3}A_{3,2} - A_{1,1}A_{12,12}A_{2,3}A_{3,2} - A_{1,12}A_{12,1}A_{2,2}A_{3,3} + A_{1,1}A_{12,12}A_{2,2}A_{3,3} + \\ & A_{12,2}(A_{1,3}A_{2,12}A_{3,1} - A_{1,12}A_{2,3}A_{3,1} - A_{1,3}A_{2,1}A_{3,12} + A_{1,1}A_{2,3}A_{3,12} + \\ & A_{1,12}A_{2,1}A_{3,3} - A_{1,1}A_{2,12}A_{3,3}) + A_{1,2}(-A_{12,3}A_{2,12}A_{3,1} + A_{12,12}A_{2,3}A_{3,1} + \\ & A_{12,3}A_{2,1}A_{3,12} - A_{12,1}A_{2,3}A_{3,12} - A_{12,12}A_{2,1}A_{3,3} + A_{12,1}A_{2,12}A_{3,3}). \end{aligned} \quad (94)$$

Appendix B

The extended Eshelby symbol appropriate to orthorhombic $mm2$ piezoelectric materials, distributed as ellipsoidal particles with shape parameters $\{a, b, c\}$, is given by [10, 32]

$$S_{MnAb}^{(esh)} = \begin{cases} \frac{1}{8\pi} C_s^{(1)} J_{Ab} \int_{-1}^{+1} d\zeta_3 \int_0^{2\pi} d\omega [F_{mJsn}(\bar{\vartheta}) + F_{nJsm}(\bar{\vartheta})], & M = m = 1, 2, 3 \\ \frac{1}{4\pi} C_s^{(1)} J_{Ab} \int_{-1}^{+1} d\zeta_3 \int_0^{2\pi} d\omega F_{4Jsn}(\bar{\vartheta}), & M = 4 \end{cases}, \quad (95)$$

wherein

$$\left. \begin{aligned} F_{MJsn}(\bar{\vartheta}) &= \bar{\vartheta}_s \bar{\vartheta}_n K_{MJ}^{-1}, & K_{JR} &= \bar{\vartheta}_s C_{sJRn}^{(1)} \bar{\vartheta}_n \\ \bar{\vartheta}_1 &= \frac{\zeta_1}{a}, & \bar{\vartheta}_2 &= \frac{\zeta_2}{b}, & \bar{\vartheta}_3 &= \frac{\zeta_3}{c} \\ \zeta_1 &= (1 - \zeta_3^2)^{1/2} \cos(\omega), & \zeta_2 &= (1 - \zeta_3^2)^{1/2} \sin(\omega), & \zeta_3 &= \zeta_3 \end{aligned} \right\}. \quad (96)$$

The integrals in eqs. (95) can be evaluated using standard numerical methods [30].

The conversion from the extended Eshelby symbol $S_{MnAb}^{(esh)}$ to the extended Eshelby 12×12 matrix, namely $\underline{\underline{\mathbf{S}}}^{(Esh)}$, follows the scheme described in Appendix A.

Acknowledgement: AJD is supported by an *Engineering and Physical Sciences Research Council* (UK) studentship.

References

- [1] Ting R Y 1986 Evaluation of new piezoelectric composite materials for hydrophone applications *Ferroelectrics* **67** 143–157
- [2] Zhang R, Jiang B and Cao W 2001 Elastic, piezoelectric, and dielectric properties of multidomain $0.67\text{Pb}(\text{Mg}_{1/3}\text{Nb}_{2/3})\text{O}_3 - 0.33\text{PbTiO}_3$ single crystals *J. Appl. Phys.* **90** 3471–3475
- [3] Damjanovic D 1998 Ferroelectric, dielectric and piezoelectric properties of ferroelectric thin films and ceramics *Rep. Prog. Phys.* **61** 1267–1324
- [4] Swallow L M, Luo J K, Siores E, Patel I and Dodds D 2008 A piezoelectric fibre composite based energy harvesting device for potential wearable applications *Smart Mater. Struct.* **17** 025017
- [5] Walser R M 2003 Metamaterials: an introduction *Introduction to Complex Mediums for Optics and Electromagnetics* eds W S Weiglhofer and A Lakhtakia (Bellingham, WA, USA: SPIE Press) pp295–316
- [6] Mackay T G 2005 Linear and nonlinear homogenized composite mediums as metamaterials *Electromagnetics* **25** 461–481
- [7] Eshelby J D 1957 The determination of the elastic field of an ellipsoidal inclusion, and related problems *Proc. R. Soc. Lond. A* **241** 376–396
- [8] Giordano S and Palla P L 2008 Dielectric behavior of anisotropic inhomogeneities: interior and exterior point Eshelby tensors *J. Phys. A: Math. Theor.* **41** 415205
- [9] Mori T and Tanaka K 1973 Average stress in matrix and average elastic energy of materials misfitting inclusions *Acta Metallurgica* **21** 571–574
- [10] Dunn M L and Taya M 1993 An analysis of piezoelectric composite materials containing ellipsoidal inhomogeneities *Proc. R. Soc.: Math. Phys. Sci.* **443** 265–287
- [11] Huang J H and Kuo W–S 1996 The analysis of piezoelectric/piezomagnetic composite materials containing ellipsoidal inclusions *J. Appl. Phys.* **81** 1378–1386
- [12] Dunn M L and Taya M 1993 Micromechanics predictions of the effective electroelastic moduli of piezoelectric composites *Int. J. Solids Structures* **30** 161–175
- [13] Odegard G M 2004 Constitutive modeling of piezoelectric polymer composites *Acta Mater.* **52** 5315–5330
- [14] Ryzhov Yu A and Tamoikin V V 1970 Radiation and propagation of electromagnetic waves in randomly inhomogeneous media *Radiophys. Quantum Electron.* **14** 228–233

- [15] Tsang L and Kong J A 1981 Scattering of electromagnetic waves from random media with strong permittivity fluctuations *Radio Sci.* **16** 303–320
- [16] Michel B and Lakhtakia A 1995 Strong–property–fluctuation theory for homogenizing chiral particulate composites *Phys. Rev. E* **51** 5701–5707
- [17] Mackay T G, Lakhtakia A and Weiglhofer W S 2000 Strong-property-fluctuation theory for homogenization of bianisotropic composites: Formulation *Phys. Rev. E* **62** 6052–6064 Erratum: 2001 **63** 049901
- [18] Zhuck N P 1996 Strong fluctuation theory for a mean acoustic field in a random fluid medium with statistically anisotropic perturbations *J. Acoust. Soc. Am.* **99** 46–54
- [19] Zhuck N P and Lakhtakia A 1999 Effective constitutive properties of a disordered elastic solid medium via the strong–fluctuation approach *Proc R. Soc. Lond. A* **455** 543–566
- [20] Duncan A D, Mackay T G and Lakhtakia A 2008 On the homogenization of orthotropic elastic composites by the strong–property–fluctuation theory [http : //arxiv.org/abs/0810.5671](http://arxiv.org/abs/0810.5671)
- [21] Nye J F 1985 *Physical Properties of Crystals* (Oxford, UK: Clarendon)
- [22] Auld B A 1990 *Acoustic Fields and Waves in Solids*, 2nd edn (Malabar, FL, USA: Krieger Publishing Company)
- [23] Mura T 1987 *Micromechanics of Defects in Solids* (Dordrecht, The Netherlands: Kluwer)
- [24] Lakhtakia A 2002 Microscopic model for elastostatic and elastodynamic excitation of chiral sculptured thin films *J. Compos. Mater.* **36** 1277–1298
- [25] Mackay T G, Lakhtakia A and Weiglhofer W S 2001 Homogenisation of similarly oriented, metallic, ellipsoidal inclusions using the bilocally approximated strong–property–fluctuation theory *Opt. Commun.* **107** 89–95
- [26] Tsang L, Kong J A and Newton R W 1982 Application of strong fluctuation random medium theory to scattering of electromagnetic waves from a half–space of dielectric mixture *IEEE Trans. Antennas Propagat.* **30** 292–302
- [27] Ma H and Wang B 2005 The scattering of electrostatic waves by an ellipsoidal inclusion in piezoelectric medium *Int. J. Solids Structures* **42** 4541–4554
- [28] Bagnara R 1995 A unified proof for the convergence of Jacobi and Gauss–Seidel methods *SIAM Review* **37** 93–97
- [29] Kwok Y K 2002 *Applied Complex Variables for Scientists and Engineers* (Cambridge, UK: Cambridge University Press)
- [30] Press W H, Flannery B P, Teukolsky S A and Vetterling W T 1992 *Numerical Recipes in Fortran*, 2nd edn (Cambridge, UK: Cambridge University Press)
- [31] Holland R 1967 Representation of dielectric, elastic, and piezoelectric losses by complex coefficients *IEEE Trans. Son. Ultrason.* **14** 18–20
- [32] Gavazzi A C and Lagoudas D C 1990 On the numerical evaluation of Eshelby’s tensor and its application to elastoplastic fibrous composites *Comp. Mech.* **7** 13–19
- [33] Willis J R 1985 The nonlocal influence of density variations in a composite *Int. J. Solids Structures* **21** 805–817
- [34] Milton G W 2007 New metamaterials with macroscopic behavior outside that of continuum elastodynamics *New J. Physics* **9** 359

- [35] Genchev Z D 1992 Anisotropic and gyrotropic version of Polder and van Santen's mixing formula *Waves Random Media* **2** 99–110
- [36] Zhuck N P 1994 Strong-fluctuation theory for a mean electromagnetic field in a statistically homogeneous random medium with arbitrary anisotropy of electrical and statistical properties *Phys. Rev. B* **50** 15636–15645
- [37] Nan C-W 1994 Magnetoelectric effect in composites of piezoelectric and piezomagnetic phases *Phys. Rev. B* **50** 6082–6088
- [38] Adler P M and Mityushev V 2003 Effective medium approximation and exact formulae for electrokinetic phenomena in porous media *J. Phys. A: Math. Gen.* **36** 391–404

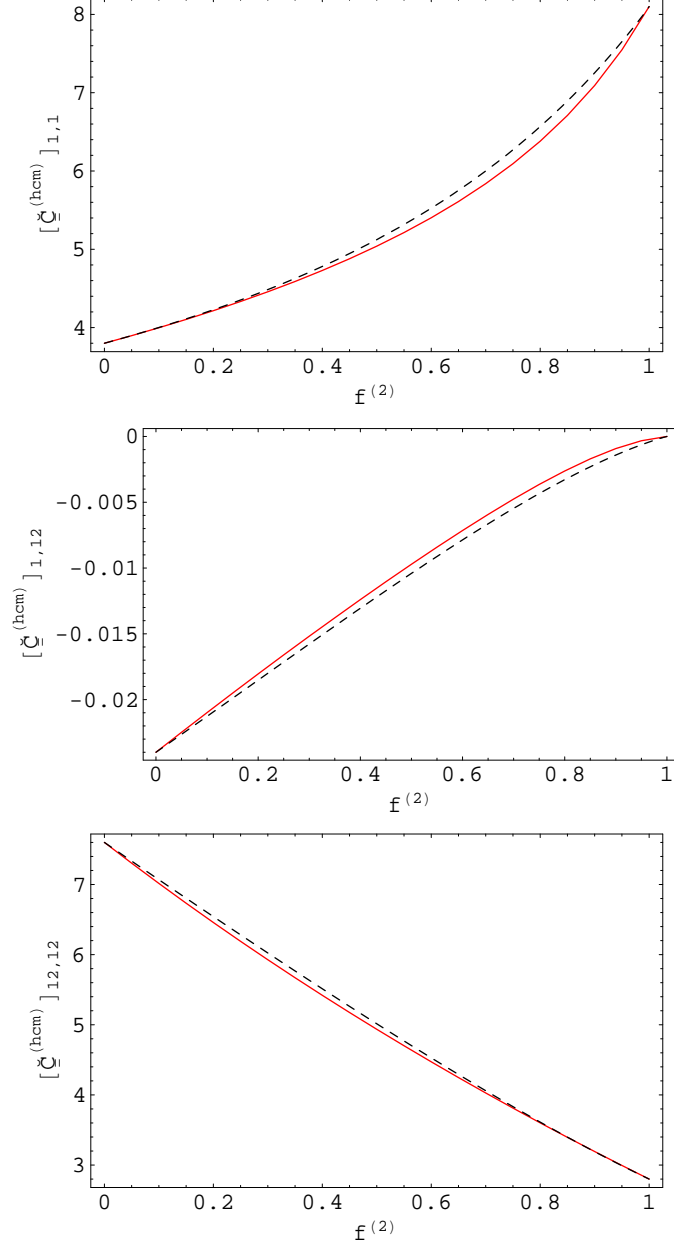


Figure 1: Plots of $[\check{\underline{C}}]_{1,1}^{(hcm)}$ (in GPa), $[\check{\underline{C}}]_{1,12}^{(hcm)}$ (in $C m^{-2}$) and $(1/\epsilon_0)[\check{\underline{C}}]_{12,12}^{(hcm)}$ as estimated using the lowest-order SPFT (i.e., $hcm = ocm$) (black, dashed curves) and the Mori-Tanaka formalism (i.e., $hcm = MT$) (red, solid curves), versus the volume fraction of component material ‘2’. Component material ‘1’ is PVDF and component material ‘2’ is LaRC-SI, as described in §3.1. The component materials are distributed as spheres (i.e., $a = b = c$).

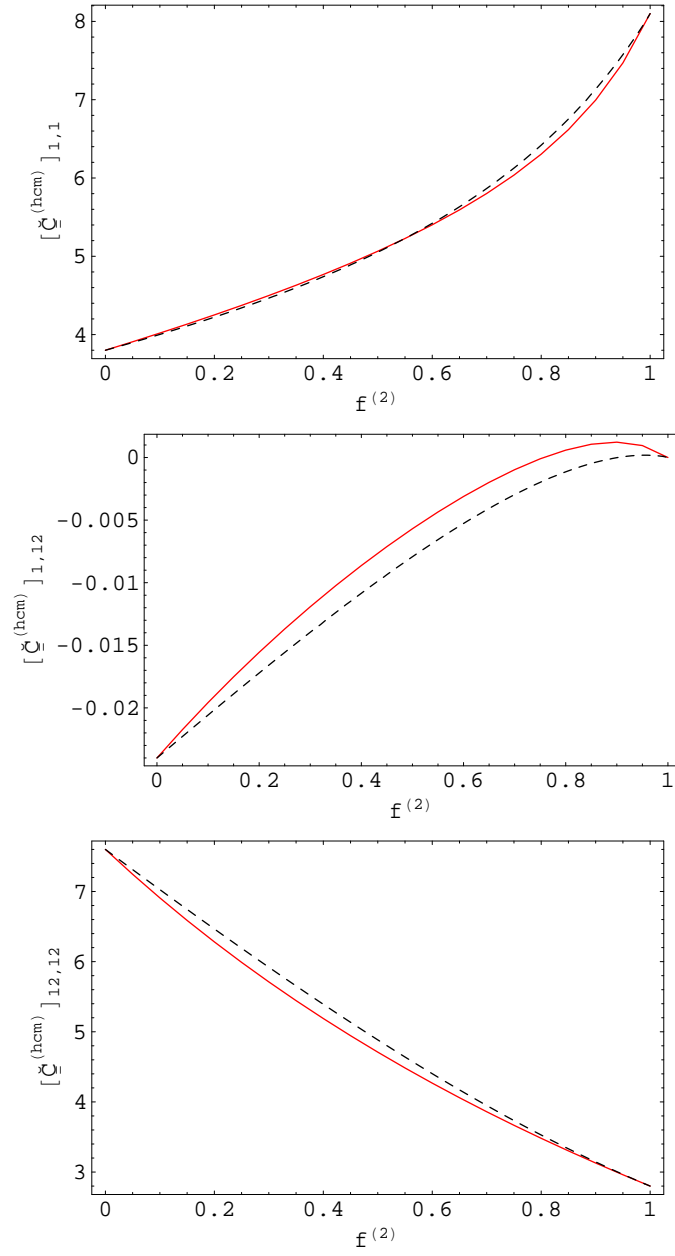


Figure 2: As Fig. 1 but with the component materials distributed as ellipsoids with $(a/c = 5$ and $b/c = 1.5)$.

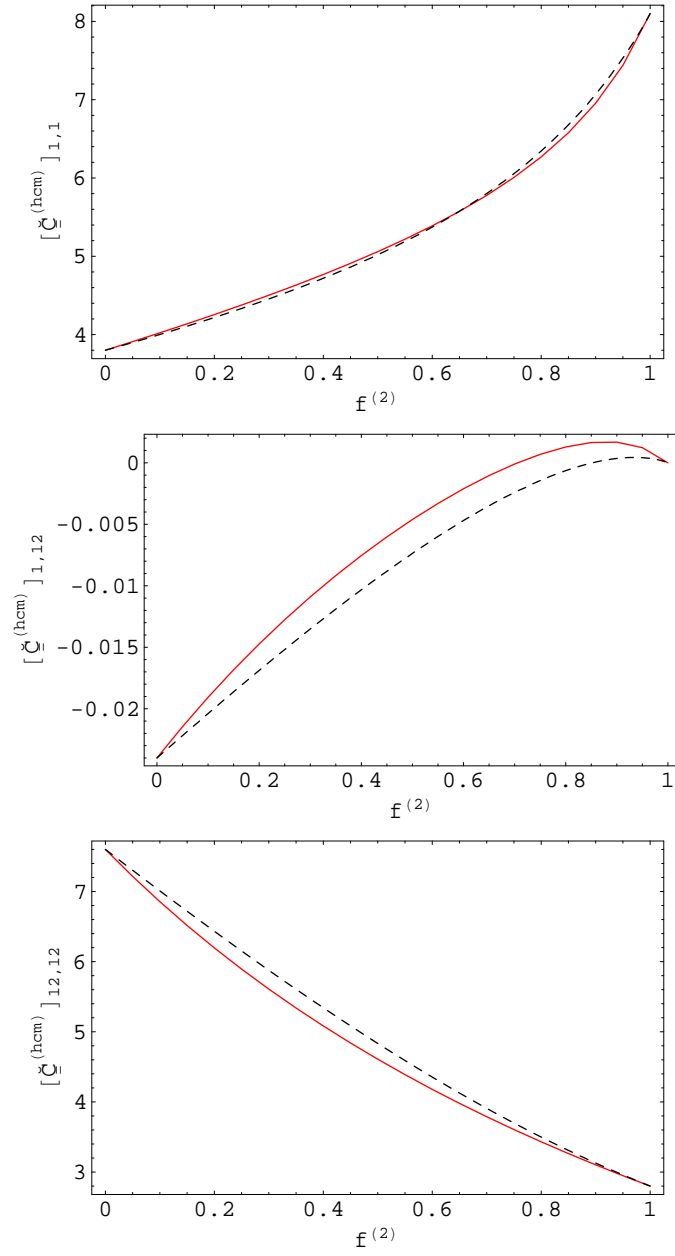


Figure 3: As Fig. 1 but with the component materials distributed as ellipsoids with $(a/c = 10$ and $b/c = 2)$.

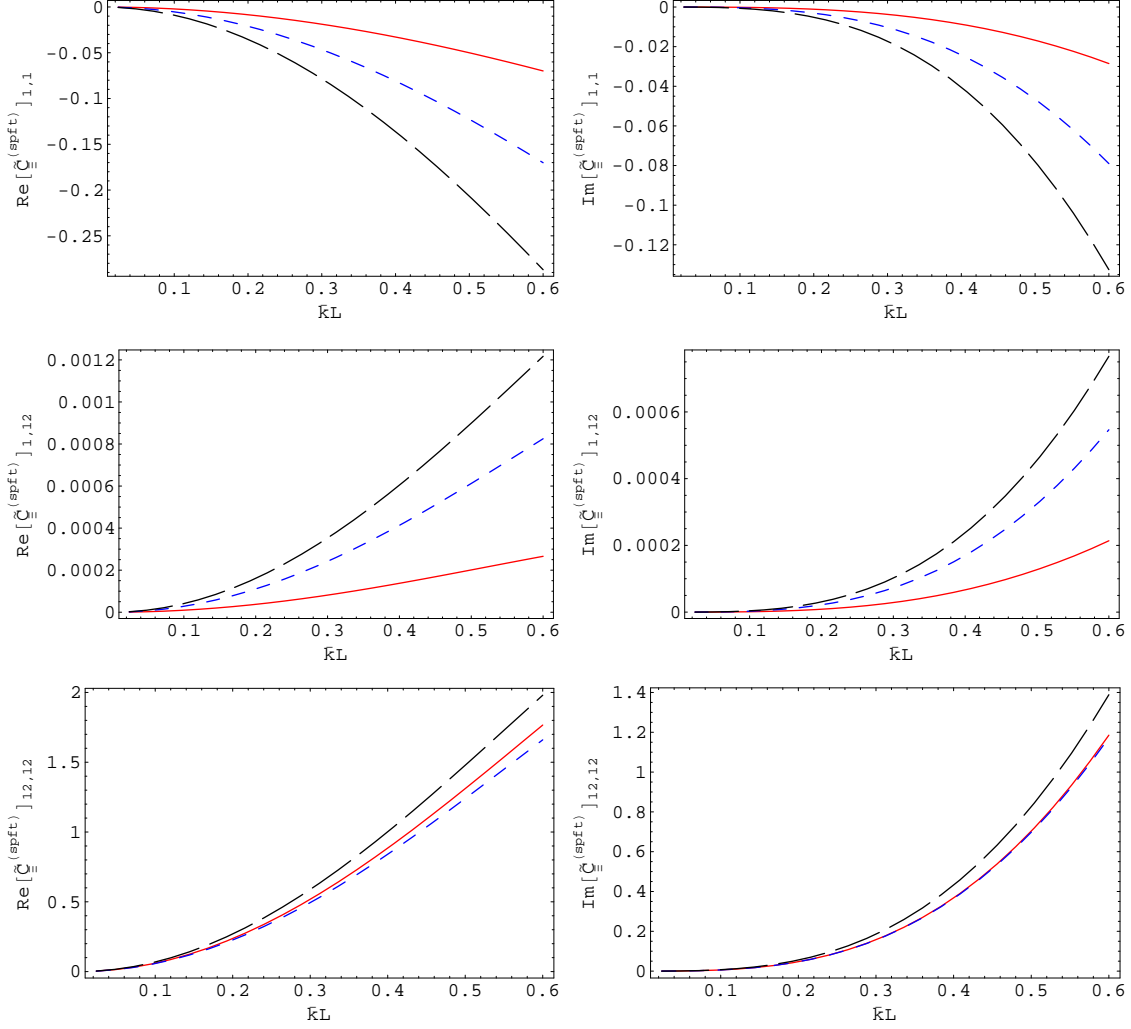


Figure 4: Plots of the real and imaginary parts of the second-order SPFT estimates $\left[\tilde{\underline{\underline{\mathbf{C}}}}^{(spft)}\right]_{1,1}$ (in GPa), $\left[\tilde{\underline{\underline{\mathbf{C}}}}^{(spft)}\right]_{1,12}$ (in C m^{-2}) and $(10^3/\epsilon_0)\left[\tilde{\underline{\underline{\mathbf{C}}}}^{(spft)}\right]_{12,12}$, where $\tilde{\underline{\underline{\mathbf{C}}}}^{(spft)} = \underline{\underline{\mathbf{C}}}^{(spft)} - \underline{\underline{\mathbf{C}}}^{(ocm)}$, versus $\bar{k}L$, with $f^{(2)} = 0.5$. The results from the spherical particle (i.e., $a = b = c = 1$) case (red, solid line) are plotted alongside the cases with elliptical particles with $a = 5, b = 1.5, c = 1$ (blue, short-dashed line) and $a = 10, b = 2, c = 1$ (black, long-dashed line). Component material ‘1’ is PVDF and component material ‘2’ is LaRC-SI, as described in §3.1.

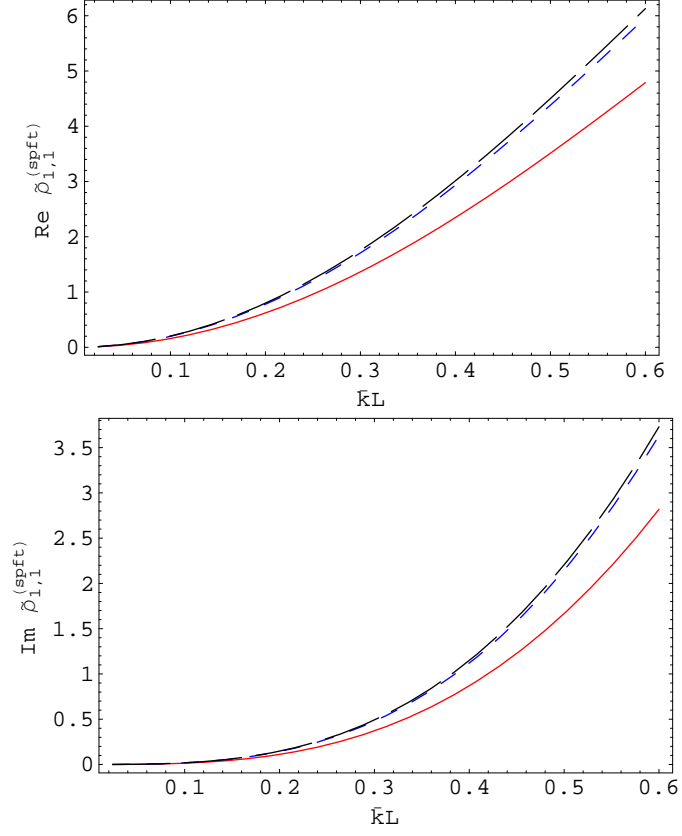


Figure 5: As Fig. 4 but with the real and imaginary parts of $\left[\tilde{\underline{\underline{\rho}}}^{(spft)}\right]_{11}$ (in kg m^{-3}), where $\tilde{\underline{\underline{\rho}}}^{(spft)} = \underline{\underline{\rho}}^{(spft)} - \underline{\underline{\rho}}^{(ocm)}$, plotted as functions of $\bar{k}L$, with $f^{(2)} = 0.5$.